Journal of Physics: Conference Series **3173** (2026) 012006 doi:10.1088/1742-6596/3173/1/012006

# Characterization of the transient response of oscillating DBD plasma actuators for turbulent skin-friction control

**L. Magnani[1], G. Neretti[3], J. Serpieri[4], A. Popoli[3], A. Cristofolini[3], A. Talamelli[1,2] and G. Bellani[1,2]**

[1]Department of Industrial Engineering (DIN), University of Bologna, Bologna, Italy
[2]Interdepartmental Centre for Industrial Research (CIRI Aerospace), University of Bologna, Forlì, Italy
[3]Department of Electrical, Electronic and Information Engineering 'Gugliemo Marconi', University of Bologna, Bologna, Italy
[4]Department of Mechanical and Aerospace Engineering(DIMEAS), Politecnico di Torino, Turin, Italy

E-mail: lorenzo.magnani9@unibo.it

**Abstract.** Controlling near-wall turbulent structures is essential to achieve significant skin-friction drag reduction. Oscillating walls have been shown to reduce friction drag caused by turbulence when actuation is tuned to turbulent time-scales, but reproducing the same flow field without moving surfaces remains a challenge. Plasma actuators based on Dielectric Barrier Discharge (DBD) provide a promising alternative, enabling wall-parallel oscillating flows without mechanical motion. To assess their performance in realistic conditions, actuator geometry and electrical parameters must be optimized for high values of Reynolds number. The CICLoPE Long Pipe facility offers a unique environment for such studies. Here, we present a characterization of the transient response of DBD plasma actuators designed for $Re_\tau > 10,000$. Using Schlieren imaging with high-speed acquisition up to $10,000\ fps$, density and temperature fronts induced by plasma actuators have been tracked. A dedicated image-processing algorithm was developed, enabling the study of wall temperature fields induced by the plasma actuator, as well as providing a reliable tracking of the plasma-induced flow and the phase-actuation symmetry.

## 1 Introduction

Reducing the aerodynamic drag of next-generation aircraft is a key objective in sustainable development plans at national, European, and international levels. To reduce friction drag, which accounts for approximately 50 % of the total drag during cruise, smart surfaces are being developed and tested. Reducing the friction drag of large airliners requires controlling turbulent fluctuations, in particular those related to the near-wall cycle [1]. Several studies demonstrated that oscillating a wall in a specific direction can lead to a significant reduction in friction drag [2]. Recent numerical studies showed a gain in drag-reduction performance by tuning the actuation time-scales on the very-large scale motions, highlighting the need of developing flow-control strategies in high-Reynolds number flow conditions [3, 4]. Another technological challenge is to approximate the Stokes layer induced by wall-oscillations with actuators that do not

require any moving surface. To this end, Dielectric Barrier Discharge plasma actuators (DBD-PA) have been developed, showing promising performances [5, 6].

To test and optimize their performance in realistic flow conditions, the geometry, actuation timing and electrical actuation parameters must be tuned based on the temporal and spatial scales of high-Reynolds number turbulent flows. The Long Pipe wind tunnel of the Centre for International Cooperation in Long Pipe Experiments (CICLoPE) provides an ideal environment for such studies: with an inner diameter equal to 0.9 $m$ and a length of 111.5 $m$, it allows precise measurements of near-wall flow fluctuations, providing a reliable baseline for evaluating smart surfaces [7].

## 2 Experimental setup

### *2.1 Plasma actuator layout*

Oscillating DBD plasma actuators are composed by two high voltage (HV) electrodes exposed to the flow and a ground (GND) electrode, separated by a dielectric material. By supplying the exposed electrodes with a sufficiently high voltage($V_{AC}$) at a given sinusoidal frequency ($f_{AC}$), free-electrons are accelerated, colliding with neutral molecules and causing ionization. On one hand, this generates new free-electrons: given their low mass, they get strongly accelerated by the electric field, triggering the Townsend avalanche process and leading to the formation of cold plasma. On the other hand, the ionization process causes the formation of (positive) ions, heavier than electrons: thus, colliding with neutral molecules, they transfer electric energy into mechanical energy, throughout the so called Electro-Hydro-Dynamic (EHD) interaction. This, in turns, generates the ionic wind and the so called Plasma Induced Flow(PIF), which develops in a wall-parallel direction (see Fig.1a).

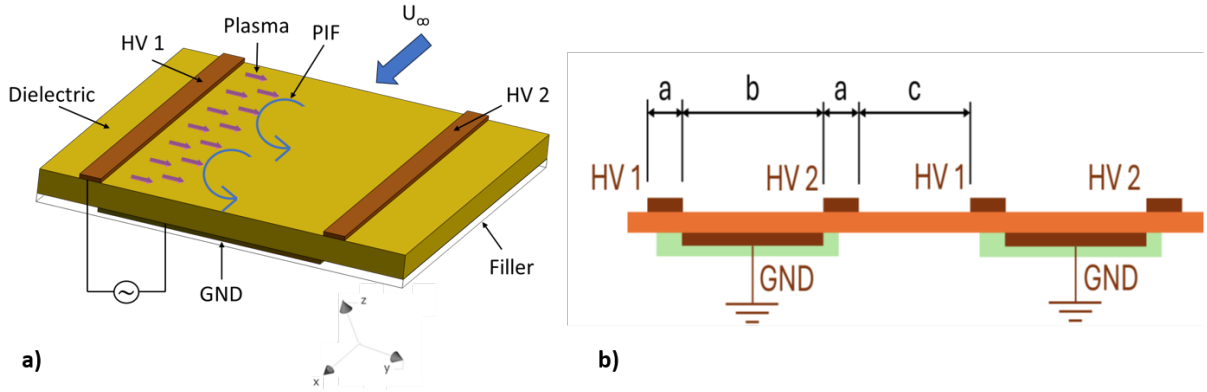


Figure 1: a) Working principle of a plasma actuator; b) Schematic of an array of oscillating plasma actuators.

To reproduce an oscillating wall-parallel flow, several pairs of actuators must be alternately turned on and off, according to a square-wave modulation signal, controlled both in frequency ($f_M$) and duty cycle.

The layout of the array of plasma actuators is depicted in Fig.1b. Each single plasma actuator is composed of a 500 $\mu m$-thick layer of Kapton interposed, as a dielectric barrier, between two high-voltage electrodes (HV 1 and HV 2) and a ground electrode, both aligned in the streamwise ($x$) direction. The high-voltage electrodes are exposed to the flow, and the ground electrode is electrically insulated with an epoxy resin to avoid undesired plasma discharges. The geometric dimensions for the present application, illustrated in Fig.1b, were chosen as:

- Exposed high-voltage electrode width: $a = 3\ mm$, chosen to avoid the formation of "back plasma", i.e. plasma in the opposite direction;
- Ground electrode width: $b = 9\ mm$, large enough to allow the full development of the plasma front and to avoid a direct surface discharge between two exposed HV electrodes;
- Inter-module spacing: $c = 6\ mm$, to avoid electrical interaction between adjacent electrodes.

### *2.2 Schlieren imaging technique*

Experiments were conducted using the Schlieren technique, which visualizes density variations induced by the PIF. Indeed, the plasma production process also causes moderate heating of the air surrounding the high-voltage electrode. The Schlieren imaging technique, exploiting the difference in the air refractive index generated by the temperature variation, allows to visualize the plasma-induced flow. Combining the Schlieren technique with high-speed imaging, time-resolved measurements on the plasma-induced flow can be performed, allowing for a detailed study of the transient-flow behavior.

Images were captured by means of a Z-type configuration Schlieren setup, coupled with a high-speed camera Phantom Miro M340, with sensor size of $2560 \times 1600$ $pixels^2$, a pixel size of 10 $\mu m$, 12-bits of digital resolution and capable of capturing up to $51,000$ images per second. For the experiments, it was used a frame rate equal to $10,000$ $fps$, corresponding to an image resolution equal to $384 \times 512$ $pixels^2$. A calibration procedure was performed, providing a spatial resolution equal to 0.071 $mm/px$; therefore, the resulting field of view, after a further cropping procedure, was approximately $28 \times 28$ $mm^2$, which was sufficient to capture the flow in between two electrodes.

An example of a Schlieren image after a background image subtraction (corresponding to the non-actuated case), along with a schematic of the plasma actuation, is shown in Fig.2; spanwise and wall-normal directions are denoted by $y$ and $z$ coordinates, respectively.

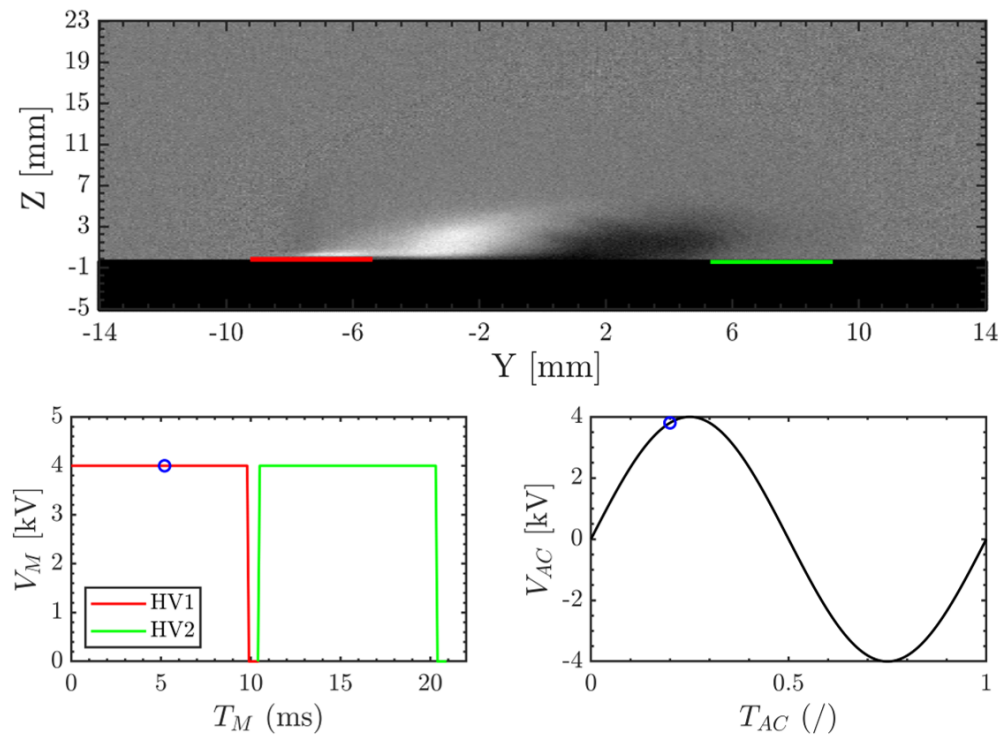


Figure 2: Example of a Schlieren image acquired with the high-speed camera at 5 $ms$ after plasma ignition: red and green markers represent, respectively, HV 1 and HV 2, while the blue circle marks the specific temporal instant in both the modulation and actuation period. The bottom-left image represents the (square) modulation signal (modulation period $T_M = 10$ $ms$), while the bottom-right image depicts the sinusoidal high-frequency signal provided by the power supply.

## 3 Methodology

To assess the evolution in time of the spanwise flow starting from the Schlieren images, an ad-hoc algorithm was implemented. In fact, assuming that the temperature field behaves as a passive scalar diffusing under the action of the plasma-induced flow, the progression of this "hot-front" can be detected. Starting from the raw images, the operation performed by the algorithm were:

- Background-image subtraction;

- definition of a Region Of Interest (ROI);
- min-max normalization of the luminosity intensity values;
- integration in the spanwise direction, according to the following relationship:

$$\int_0^y I(y', z)dy' \propto \Delta x \int_0^y \frac{\partial \rho(y', z)}{\partial y'} dy' \ , \tag{1}$$

where $I$ represents the light intensity collected by the high-speed camera, $\rho$ is the air density, and $x, y, z$ denote the streamwise, spanwise and wall-normal direction, respectively.

This last operation was performed because, since density gradients are generated by a temperature gradient, by integrating each frame in a direction perpendicular to the knife-edge orientation, it is possible to retrieve a value that can be viewed as a measure of the temperature-gradient field above the actuator surface.

## 4 Results and discussion

Plasma actuators were tested applying the following parameters:

- Input voltage $V_{AC} = 4\ kV$;
- Frequency $f_{AC} = 31\ kHz$;
- Camera frame rate $10,000\ fps$;
- Modulation period $T_M$ from 5 to 80 $ms$ ($12.5 < f_{act} < 200\ Hz$);

### *4.1 Temperature-velocity profiles comparison*

In a Schlieren experiment, comparing temperature profiles with velocity profiles provides valuable insight into the coupling between thermal and aerodynamic effects induced by the actuator. Their correlation allows to assess the relative contributions of thermal forcing and momentum transfer, and to delineate the spatial extent of the interaction region. Moreover, such a comparison can be interpreted in light of the Reynolds analogy, which relates heat and momentum transfer at the wall. Indeed, similarities between the two profiles may suggest a coupled transport mechanism, whereas discrepancies may highlight different underlying driving mechanisms.

The wall-normal velocity profile induced by the PIF was measured using a 1 $mm$ glass Pitot tube, placed 2 mm downstream of the plasma front. Based on previous measurements, both the plasma extension and the corresponding induced velocity profile under the considered actuation conditions were characterized. The plasma extension was found to be approximately 3 $mm$, while the induced velocity profile is reported in Fig.3b (blue dashed line).

To ensure consistency with the Pitot measurements, the wall-normal temperature profiles were derived by analyzing the temperature field (obtained by applying the procedure described in Section 3) at the same spanwise location, that is approximately 5 $mm$ distant from the HV 1 actuator edge. Furthermore, the selected temperature field corresponds to a time instant well after the plasma-induced flow had reached its steady state.

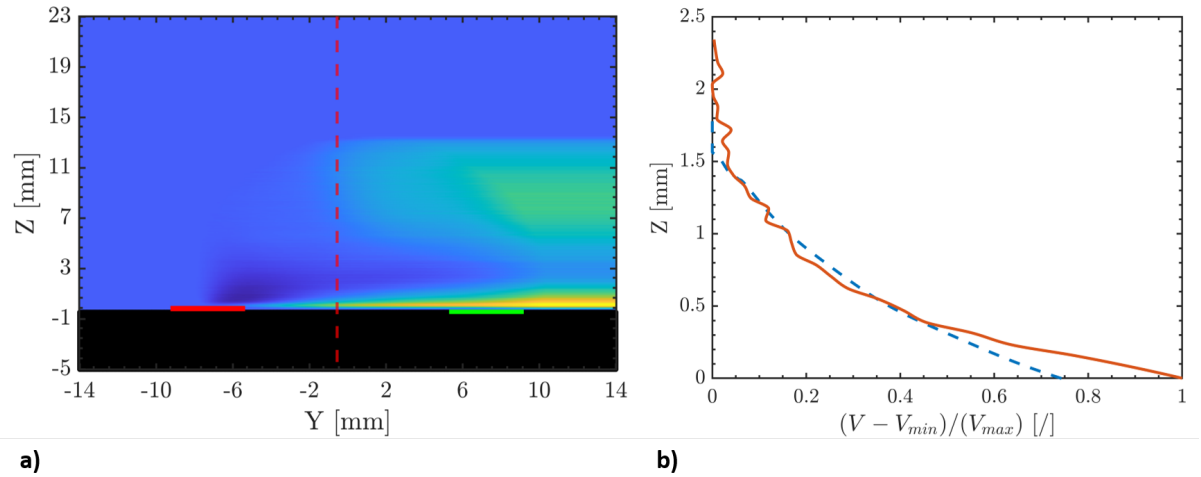


Figure 3: Comparison between wall-normal temperature and velocity profiles. a) temperature field acquired after $\approx 40\ ms$ after HV 1 ignition (dashed line represents the spanwise location of the temperature profile); b) Normalized velocity (dashed line) and temperature (solid line) wall-normal profiles.

The velocity and temperature profiles show good overall agreement, although they do not match perfectly. This discrepancy mainly arises because the Pitot measurements are time-averaged, while the temperature field represents an instantaneous Schlieren snapshot which was additionally averaged along the streamwise direction. Other factors may also play a role, such as the inherent difficulty in defining the plasma front at a macroscopic level, and the fact that the temperature profiles are obtained through an additional averaging procedure along the streamwise direction, which accounts for the effects occurring along the length of the high-voltage electrodes. Moreover, the velocity profile shown in Fig.3b results from ensemble averages of five independent acquisitions performed under comparable operating conditions (with relative standard deviations remaining below 5 %).

### *4.2 Phase-symmetry*

In order to create a robust hot-front tracking algorithm, after the integration procedure, the images were averaged column-wise in a region very close to the actuator surface, and its evolution over time was analyzed to determine the hot-front displacement. Spanwise displacement profiles of the PIF generated by HV 1 and HV 2, for different modulation periods, are shown in Figure 4:

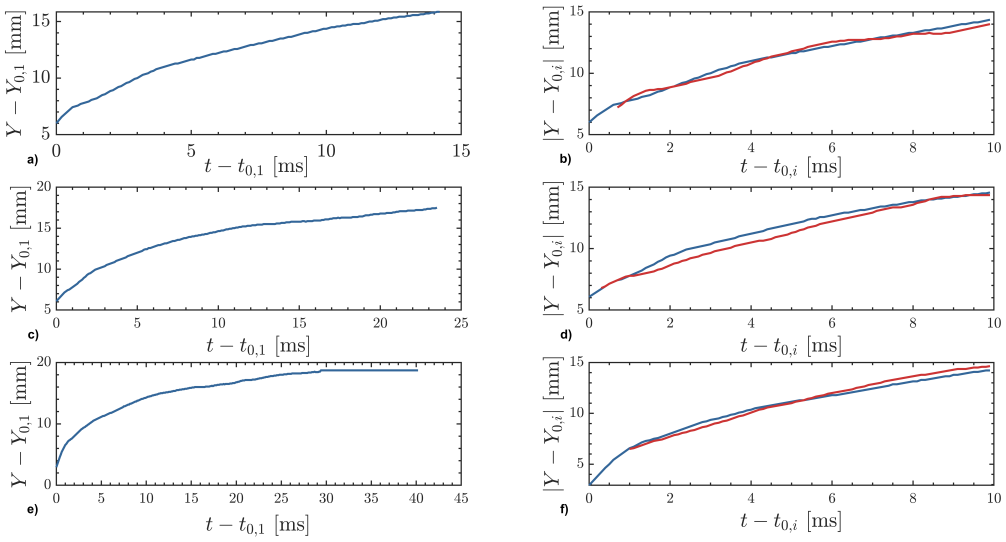


Figure 4: Spanwise front-displacement of the tangential vortex for different modulation periods (respectively $15, 25, 40$ $ms$). a,c,e): front displacement generated by HV 1 only; b,d,f): front displacement generated by both HV 1 (blue) and HV 2 (red).

The PIF is characterized by a strong initial acceleration, due to the sharp but highly localized impulse at the actuator edge; then, over time the flow diffuses, progressively decelerating up to a steady-state regime after $\approx 6$ $ms$. It should be noted that the layout of the plasma actuator was specifically designed to mimic the effect of an oscillating wall by alternately activating the two high-voltage electrodes. Consequently, the vortex generated by HV 2 develops in a region already perturbed by the previous phase. This introduces the so-called "dead-time" of approximately 1 $ms$, which accounts for uncertainties in tracking the hot-vortex front, as well as non-ideal switching effects and any parasitic discharges occurring during phase alternation.

Moreover, apart from the initial instants after modulation switching, it is possible to see that there is a certain degree of symmetry between the two phases, confirming that both phases can generate a similar induced flow. The discrepancies between the average profiles of the HV 1- and HV 2- induced jets may arise from some differences in the copper tracks' layout of the hand-made plasma actuator. However, these data confirm that plasma actuators are suitable for interacting with the small scales of turbulence.

## 5 Conclusions and future work

To reproduce the skin-friction drag reduction obtained by an oscillating wall, but without moving parts, an array of DBD plasma actuators has been developed and tested. High-speed Schlieren images were acquired at $10,000$ $fps$.

Since the velocity of the plasma-induced flow and the modulation frequency of the actuators are inherently related to the characteristic velocity and time scales of the near-wall turbulent structures they are intended to interact with, it is essential to characterize their transient response rather than only the steady-state plasma-induced flow. Therefore, first step to characterize their transient response, was to develop an image-processing algorithm, capable of tracking the plasma-induced flow in the spanwise direction. Displacement profiles showed that the plasma-induced flow is characterized by a strong initial acceleration, and a steady-state regime was reached after $\approx 6$ $ms$; moreover, the similarity between the displacement profiles of HV 1 and HV 2 proved that both phases are capable of producing comparable induced flows.

The comparison between wall-normal temperature and velocity profiles both provided a validation of the image-processing algorithm and supported supported the evidence of the Reynolds analogy at the wall.

Future experimental campaigns will focus on testing the plasma actuators inside the Long Pipe wind tunnel, also with different dielectric materials (teflon); in addition, Stereo-PIV (S-PIV) will be employed

both to acquire velocity profiles with higher resolution and to assess and quantify the effectiveness of these actuators in reducing the skin-friction drag.

**Acknowledgment**

- The work of Alessandro Talamelli was carried out within the MOST – Sustainable Mobility National Research Center and received funding from the European Union Next-GenerationEU [PIANO NAZIONALE DI RIPRESA E RESILIENZA (PNRR) – MISSIONE 4 COMPONENTE 2, INVESTIMENTO 1.4 – D.D.1033 17/06/2022, CN00000023];
- The work of Jacopo Serpieri and Arturo Popoli was carried out within the "WAll-Turbulence Active COntrol" project – funded by European Union – Next Generation EU within the PRIN 2022 PNRR program (D.D.1409 del 14/09/2022 Ministero dell'Università e della Ricerca).

**References**

[1] Pierre Ricco, Martin Skote, and Michael A. Leschziner. A review of turbulent skin-friction drag reduction by near-wall transverse forcing. *Progress in Aerospace Sciences*, 123:100713, 2021.

[2] Maurizio Quadrio. Drag reduction in turbulent boundary layers by in-plane wall motion. *Philosophical transactions. Series A, Mathematical, physical, and engineering sciences*, 369:1428–42, 04 2011.

[3] Dileep Chandran, Andrea Zampiron, A. Rouhi, Matt fu, David Wine, B. Holloway, Alexander Smits, and I. Marusic. Turbulent drag reduction by spanwise wall forcing. part 2. high-reynolds-number experiments. *Journal of Fluid Mechanics*, 968, 07 2023.

[4] Rahul Deshpande, Aman G. Kidanemariam, and Ivan Marusic. Pressure drag reduction via imposition of spanwise wall oscillations on a rough wall. *Journal of Fluid Mechanics*, 979:A21, 2024.

[5] Rasool Erfani, Hossein Zare-Behtash, Craig Hale, and Konstantinos Kontis. Development of dbd plasma actuators: The double encapsulated electrode. *Acta Astronautica*, 109:132–143, 2015.

[6] Gabriele Neretti, Andrea Cristofolini, Carlo Borghi, Alessandro Gurioli, and Roberto Pertile. Experimental results in dbd plasma actuators for air flow control. *IEEE Transactions on Plasma Science - IEEE TRANS PLASMA SCI*, 40:1678–1687, 06 2012.

[7] Alessandro Talamelli, Franco Persiani, Jens Fransson, Per-Henrik Alfredsson, Arne Johansson, Hassan Nagib, Jean-Daniel Rueedi, Katepalli Sreenivasan, and Peter Monkewitz. Ciclope - a response to the need for high reynolds number experiments. *Fluid Dynamics Research*, 41, 04 2009.